Role of alloying in the phonon and thermal transport of SnS-SnSe across the phase transition

Niuchang Ouyang,[1] Chen Wang,[1] and Yue Chen[1,2*]

1 *Department of Mechanical Engineering, The University of Hong Kong, Pokfulam Road, Hong Kong SAR, China*

2 *HKU Zhejiang Institute of Research and Innovation, 1623 Dayuan Road, Lin An 311305, China*

* yuechen@hku.hk

Abstract

Atomic-level investigations of the underlying phonon and thermal transports of strongly anharmonic alloy-based thermoelectric materials and their structural phase transitions are yet to be fully explored. Herein, we systematically investigate the anharmonic lattice dynamics and thermal transport of $SnS_{0.75}Se_{0.25}$ using perturbation theory up to quartic anharmonicity and molecular dynamics simulations with the first-principles-based machine-learning potential. We find the non-monotonic temperature dependence of the phonon linewidths and frequencies of the Γ_4 and Y_1 modes. This work demonstrates an apparent κ_L reduction from SnS to $SnS_{0.75}Se_{0.25,}$ mainly attributed to the enhanced scattering rates of the middle-frequency phonons and the decreased group velocities of the high-frequency phonons. We also find that the effects of the quartic anharmonicity on the thermal transport of SnS and $SnS_{0.75}Se_{0.25}$ are significant, and the phonon coherence contributions are non-negligible in describing the thermal transport. Moreover, we reveal a decrease of κ_L in $SnS_{0.75}Se_{0.25}$ by randomizing Se atoms, which can be ascribed to an additional phonon scattering arising from sublattice mass disorder.

1. Introduction

Atomic-level understanding of the thermal conduction in crystalline materials with low lattice thermal conductivity κ_L plays a vital role in various science and technology fields, including thermal management[1, 2] and thermoelectricity[3, 4]. In particular, a high figure of merit (zT) value is achieved by reducing κ_L for thermoelectric materials[5]. Although many experimental results [6-8] demonstrate that κ_L can be significantly reduced by alloying, the underlying thermal transport mechanism is still not fully revealed due to the lack of suitable phonon-based description. The validity of the phonon quasiparticle picture adopted in the conventional phonon-gas model (PGM) is controversial in complex alloying systems with a structural phase transition mainly due to the presence of lattice instabilities and high-order anharmonicity. Recently, SnSe is considered as a promising thermoelectric material[9-11] with $zT \approx 2.6$ at 923 K due to its intrinsic low κ_L. Despite sharing similar chemical compositions, the binary chalcogenide SnS, an analogue compound of SnSe, has only demonstrated $zT \approx 0.8$ at 875 K[6] due to a relatively high κ_L. $SnS_{0.91}Se_{0.09}$ alloy was shown by He *et al* [6] to have a suppressed thermal conductivity, whereas, the thermal transport mechanism of Se-alloyed SnS is yet to be fully investigated. Therefore, it is of great importance to study the Se-alloyed effects on the phonon properties of SnS to better understand thermal transport. In addition, it is challenging to deal with the strong anharmonicity across the structural phase transition of Se-alloyed SnS within the perturbative framework, which prevents the extraction of the temperature-dependent phonon properties. Thus, a thorough investigation of the temperature-dependent phonon spectra with a nonperturbative treatment of the anharmonic effects is of great importance to better understand the phonon transport of Se-alloyed SnS across the phase transition.

In recent years, theoretical calculations have demonstrated that temperature-dependent phonon frequency renormalization[12] and high-order phonon scattering[13-15] play indispensable roles in κ_L reduction for strongly anharmonic materials. Although the thermal transport properties of SnS[16, 17] have been calculated with the perturbation

theory (PT) up to the third order by solving the Boltzmann transport equation (BTE)[18], the role of fourth-order anharmonicity in suppressing κ_L of SnS and Se-alloyed SnS is not yet ascertained. Moreover, besides the particle-like contributions, the coherence effects dominated by wave-like phonons of Se-alloyed SnS across the phase transition are not yet explored. Therefore, an in-depth investigation of the impacts of quartic anharmonicity and phonon coherence contribution on κ_L is of great importance to better understand the heat transport mechanisms in Se-alloyed SnS.

In this work, the lattice dynamical evolution of the structural phase transition between *Pnma*-$SnS_{0.75}Se_{0.25}$ and *Cmcm*-$SnS_{0.75}Se_{0.25}$ is reproduced via molecular dynamics (MD) simulations[19] with machine learning moment tensor potentials (MTPs)[20]. The temperature-dependent phonon properties of the zone center Γ_4 and the zone boundary Y_1 modes, which drive the phase transition of $SnS_{0.75}Se_{0.25}$, are extracted from MD simulations using the normal-mode-decomposition technique[21, 22]. We reveal that the κ_L reduction after Se alloying can be attributed to the enhanced scattering rates of the middle-frequency phonons and the decreased group velocities of the high-frequency phonons. We find the effects of the quartic anharmonicity on the thermal transport of SnS and $SnS_{0.75}Se_{0.25}$ to be significant, and the phonon coherence contributions to the thermal transport of the high-temperature *Cmcm* phase to be non-negligible based on the unified theory (UT) model[23]. We also find a noticeable decrease of κ_L of $SnS_{0.75}Se_{0.25}$ at room temperature by introducing randomized Se atoms in the supercell, which can be attributed to an additional phonon scattering owing to the sublattice mass disorder.

2. Method

Non-spin polarized density functional theory (DFT) calculations for both phases of $SnS_{0.75}Se_{0.25}$ were performed using the Vienna *Ab initio* Simulation Package (VASP)[24] with the employment of the projector augmented wave (PAW)[25] method. The PBEsol[26] exchange-correlation functional was applied for all VASP calculations. A

plane wave energy cutoff of 500 eV and an energy convergence criterion of 10^{-8} eV were set in the electronic self-consistent calculations. A Monkhorst-Pack *k*-mesh[27] of 3×2×3 was used to sample the Brillouin-zone of the 128-atom supercells of the ordered $SnS_{0.75}Se_{0.25}$ and the general special quasi-random structure (SQS) of $SnS_{0.75}Se_{0.25}$. The randomization of Se atoms was generated using the general SQS algorithm[28], as implemented in Universal Structure Predictor: Evolutionary Xtallography (USPEX)[29] by mixing 16 Se atoms with 48 S atoms in a 128-atom supercell, as shown in Figure 1(b). The ordered $SnS_{0.75}Se_{0.25}$ was obtained based on a unit cell of the *Pnma*-phase, as demonstrated in Figure 1(a).

All equilibrium MD simulations were carried out using LAMMPS packages[30] with machine learning MTPs. To investigate the lattice evolution of $SnS_{0.75}Se_{0.25}$ across the structural phase transition, the temperature-dependent lattice constants and the fractional atomic coordinates were computed by averaging a corresponding MD trajectory of a 6912-atom supercell with 200 ps under the *NPT* and the *NVT* ensembles, respectively. The duration of each MD simulation of the ordered $SnS_{0.75}Se_{0.25}$ with a supercell size of 6912 atoms was 1 ns with a timestep of 1 fs at a temperature range from 100 to 900 K. The atomic velocities and positions were collected every 10 fs under the *NVE* ensemble. The power spectra were decomposed by projecting the atomic velocities onto the temperature-dependent phonon eigenvectors using the normal-mode-decomposition technique[31-34] and fitted with the Lorentzian function to obtain the phonon frequencies and linewidths.

To calculate the temperature dependencies of κ_L for SnS and the ordered $SnS_{0.75}Se_{0.25}$ based on the PT by solving the BTE[35], the renormalized second-order force constants were extracted using the temperature-dependent effective potential (TDEP)[36] scheme, as implemented in hiPhive[37]. Meanwhile, to obtain accurate temperature-dependent cubic and quartic force constants, the harmonic contributions were subtracted from the force-displacement data before training the cluster space[38]. Converged neighbour cutoff distances (2^{nd}: 7.0 Å; 3^{rd}: 5.0 Å; 4^{th}: 3.5 Å) for both SnS and the ordered

$SnS_{0.75}Se_{0.25}$ were applied to extract the temperature-dependent force constants. The contribution from the population term (κ_p) of the heat-flux operator was calculated under the single-mode relaxation time approximation (SMRTA) by solving the BTE[35]. The coherence term (κ_c) of the heat-flux operator was evaluated following the UT proposed by Simoncelli *et al.*[23] based on SMRTA. Additionally, the temperature-dependent κ_L of the ordered $SnS_{0.75}Se_{0.25}$ and the general SQS of $SnS_{0.75}Se_{0.25}$ were calculated using non-equilibrium molecular dynamics (NEMD)[39] simulations combined with the machine learning MTPs.

3. Results and discussion

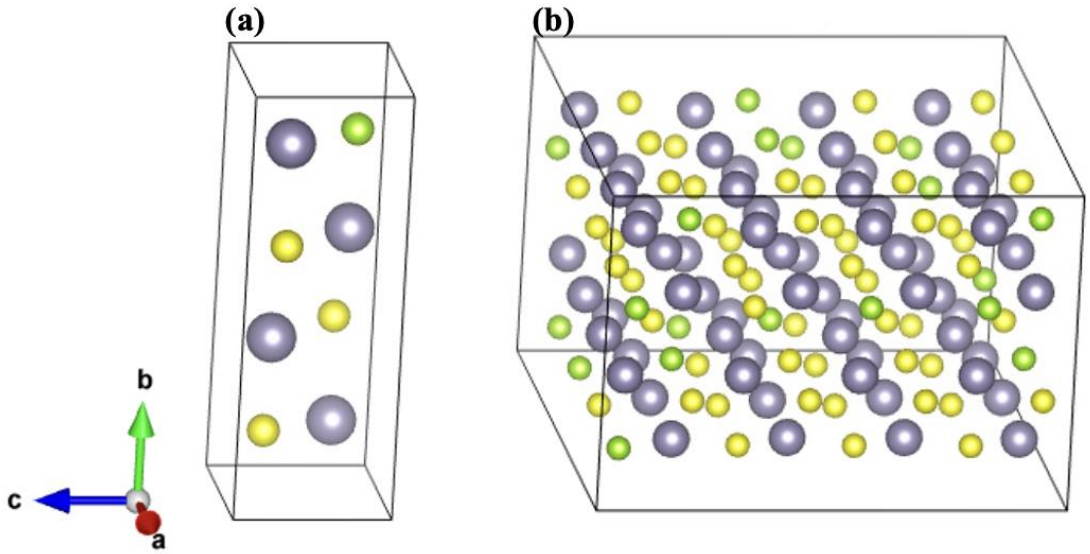

Figure 1. (a) The ordered *Pnma*-$SnS_{0.75}Se_{0.25}$ obtained based on a unit cell, which is visualized by VESTA[40]. (b) The general SQS of *Pnma*-$SnS_{0.75}Se_{0.25}$ with 128 atoms generated by USPEX[29], where Sn atoms are purple, S atoms are yellow and Se atoms are green.

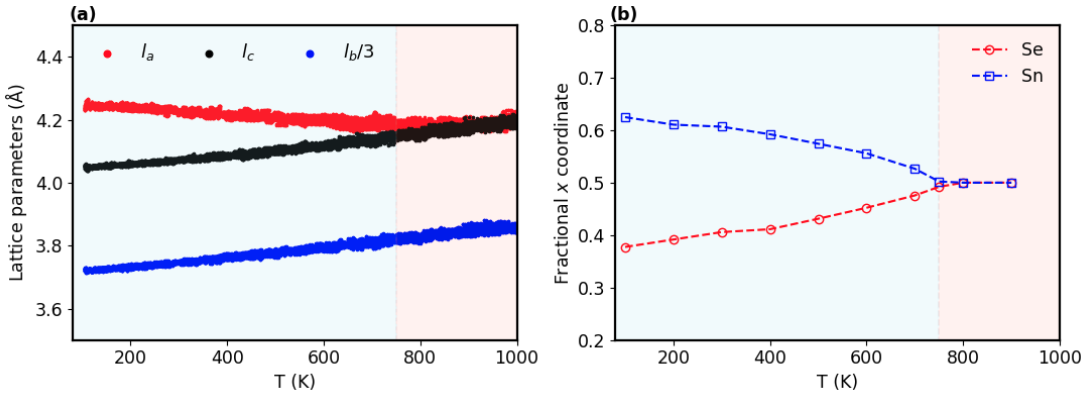

Figure 2. (a) Evolution of the lattice constants of the ordered $SnS_{0.75}Se_{0.25}$ as a function of temperature obtained from MD simulations under *NPT* ensemble at a heating rate of 4.5 K per ps. (b) The fractional atomic coordinates of the ordered $SnS_{0.75}Se_{0.25}$ in the conventional unit cell along *a* axis obtained from MD simulations under *NVT* ensemble at different temperatures. The light blue and red shaded areas stand for the *Pnma*-$SnS_{0.75}Se_{0.25}$ and *Cmcm*-$SnS_{0.75}Se_{0.25}$ phases, respectively, based on our MD simulations.

The thermal structural evolution of the ordered $SnS_{0.75}Se_{0.25}$ across the structural phase transition is interpreted by calculating the variation of the lattice constants from 100 to 1000 K, as shown in Figure 2(a). The difference of lattice constants between *a* and *c* axes calculated with our MTPs decreases continuously with increasing temperature and disappears at about T_c = 750 K for the ordered $SnS_{0.75}Se_{0.25}$, showing a similar phase transition behaviour with previous theoretical and experimental studies of SnS and SnSe[41-43]. The subtle difference in lattice constants between the ordered $SnS_{0.75}Se_{0.25}$ and the general SQS of $SnS_{0.75}Se_{0.25}$ (see Supporting Information Figure S10) reveals that introducing sublattice mass disorder has little effect on the lattice parameters across the structural phase transition. The evolution of the fractional coordinates of Sn and Se atoms in the ordered $SnS_{0.75}Se_{0.25}$ along *a* axis from 100 to 900 K is shown in Figure 2(b). The discrepancy between the Sn and Se atomic fractional coordinates decreases continuously and vanishes above 750 K, illustrating a displacive character and a higher structural symmetry across the phase transition, which is consistent with previous experimental reports of SnSe[41-43]. These results manifest that our MTPs can successfully capture the temperature-dependent lattice evolution of the ordered and the general SQS of $SnS_{0.75}Se_{0.25}$ across the structural phase transition.

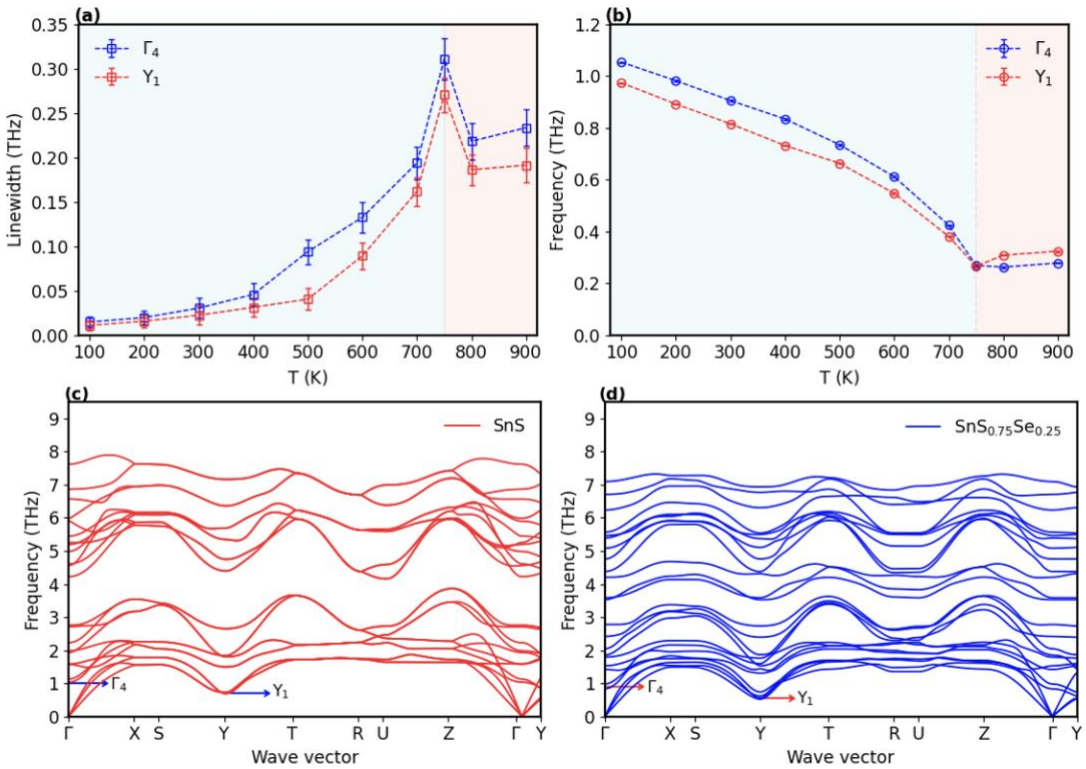

Figure 3. Temperature-dependent phonon linewidths (a) and frequencies (b) of the zone center Γ_4 and the zone boundary Y_1 modes of the ordered $SnS_{0.75}Se_{0.25}$ obtained from MD simulations. The error bars were calculated based on four independent MD simulations under the *NVE* ensemble with a duration of 1 ns for each temperature. The error bar was calculated through the standard deviation function: $\sigma = \sqrt{\frac{1}{N}\sum_{i=1}^{N}(y_i - u)^2}$, where y_i is the phonon linewidth or frequency, u is the mean value of y_i, and N is the number of independent simulations. The light blue and red shaded areas represent the ordered *Pnma*-$SnS_{0.75}Se_{0.25}$ and *Cmcm*-$SnS_{0.75}Se_{0.25}$ phases, respectively. Renormalized phonon dispersions of the *Pnma* phase of SnS (c) and the ordered $SnS_{0.75}Se_{0.25}$ (d) at 300 K calculated using the TDEP method[36] via hiPhive[44]. The subscripts of Γ_4 and Y_1 denote the mode numbers in order of increasing phonon frequency.

To investigate the phonon properties of the ordered $SnS_{0.75}Se_{0.25}$ across the structural phase transition, we have calculated the frequencies and linewidths of two phonon modes related to the structural phase transition, Γ_4 at the zone center and Y_1 at the zone boundary. The subscripts denote the number of the corresponding phonon modes in the order of increasing phonon frequency. The power spectra are obtained by calculating the Fourier transforms of the velocity autocorrelation functions from MD simulations[45], which are then fitted with a Lorentzian function to calculate the

temperature-dependent phonon frequencies and linewidths, as shown in Figure 3 (a-b). The frequency of Γ_4 decreases rapidly from around 1.05 THz at 100 K to about 0.26 THz near T_c = 750 K. The phonon linewidth of Γ_4 exhibits a non-monotonic temperature dependence, with a maximum value of 0.31 THz observed near T_c, demonstrating a drastically increased phonon-phonon scattering across the phase transition. We also observe similar temperature dependencies of linewidth and frequency of the Y_1 mode.

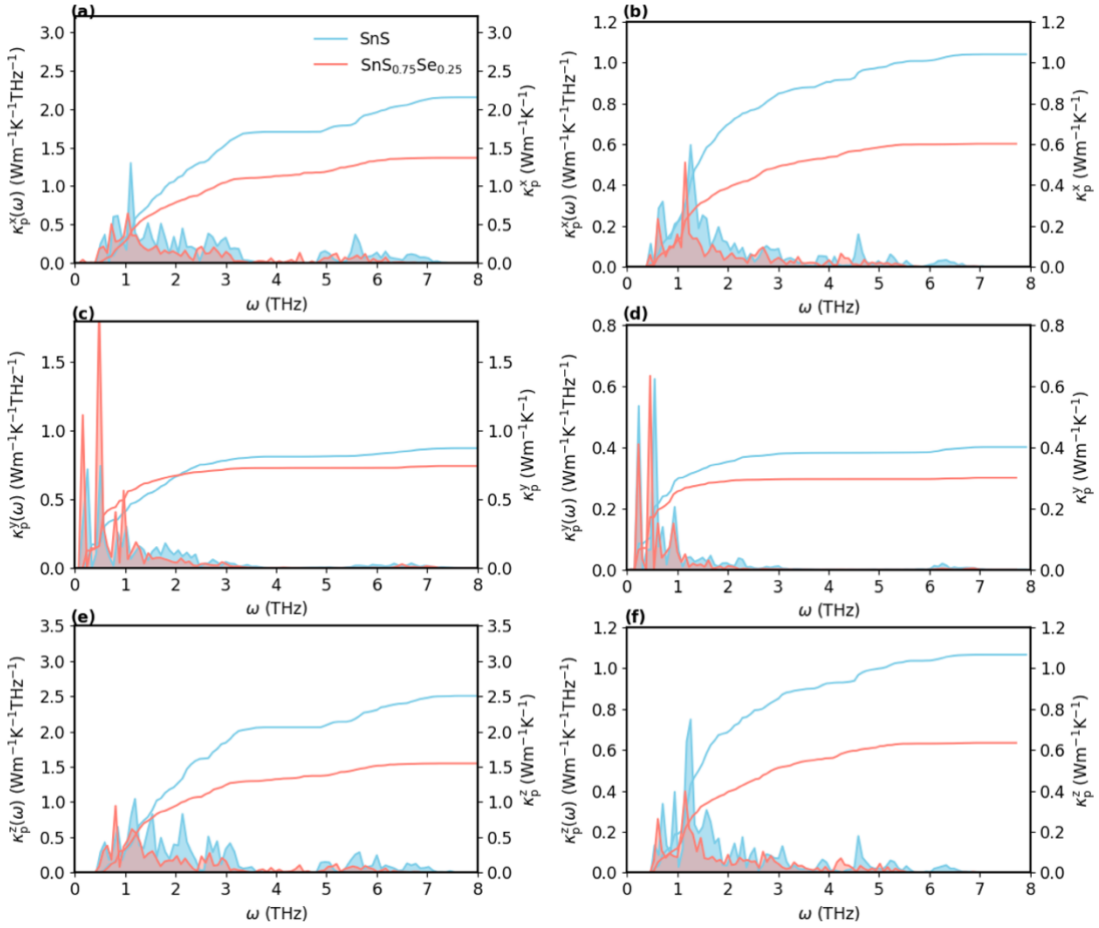

Figure 4. The differential and cumulative κ_p along three lattice directions as a function of the phonon frequency of SnS and the ordered $SnS_{0.75}Se_{0.25}$ calculated with BTE at 300 (a, c and e) and 800 K (b, d and f).

To better understand the origin of the apparent κ_L reduction of $SnS_{0.75}Se_{0.25}$ compared to SnS, we have calculated the differential and cumulative κ_p along three lattice

directions with respect to the phonon frequency from BTE at 300 and 800 K considering both three- and four-phonon interactions, as shown in Figure 4. The calculated κ_p decreases, respectively, from 2.15, 0.87 and 2.50 $Wm^{-1}K^{-1}$ to 1.36, 0.74 and 1.54 $Wm^{-1}K^{-1}$ along *x*, *y* and *z* directions by replacing 25% S atoms with Se in the convention unit cell of *Pnma*-SnS. Besides, the average κ_p reduces from 0.81 $Wm^{-1}K^{-1}$ for *Cmcm*-SnS to 0.50 $Wm^{-1}K^{-1}$ for *Cmcm*-$SnS_{0.75}Se_{0.25}$ at 800 K (see Supporting Information Figure S6), illustrating Se-alloying causes a noticeable decrease of κ_p for both *Pnma*-SnS and *Cmcm*-SnS. The contribution of the optical phonons to the total κ_p of SnS is around 58% at 300 K, which is larger than the acoustic phonons. The high contribution from the optical phonons to κ_p can be attributed to the high group velocities, as shown in Figure 5(b). In addition, κ_p^x and κ_p^z of SnS decrease significantly in the middle-frequency region (1.5-3.5 THz) by introducing 25% Se atoms. The renormalized phonon dispersions of the ordered $SnS_{0.75}Se_{0.25}$ calculated using the TDEP method[36] show apparent softening compared with SnS, as shown in Figure 3 (c-d). The softening of middle-frequency optical phonons enhances the three-phonon scattering rates, leading to a κ_p reduction, as shown in Figure 5(a). Besides, a decrease of κ_p is also observed from Figure 4 for the high-frequency phonons (4.5-7.5 THz) in the Se-alloyed SnS. This decrease of κ_p in the high-frequency region is caused by the decreased group velocities, as shown in Figure 5(b). The effect can be further understood by the decrease in the participation ratios of Se-alloyed SnS, which leads to a stronger phonon localization (see Figure S7).

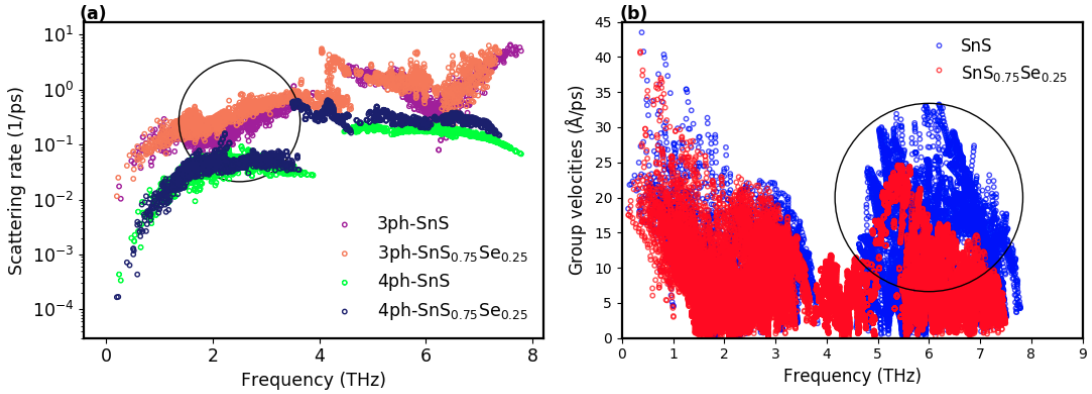

Figure 5. The phonon scattering rates (a) of SnS and the ordered $SnS_{0.75}Se_{0.25}$ calculated from PT considering three- and four-phonon scatterings at 300 K. The group velocities (b) of SnS and the ordered $SnS_{0.75}Se_{0.25}$ calculated with the renormalized second-order force constants at 300 K. The black circles highlight the large differences of scattering rates and group velocities between SnS and the ordered $SnS_{0.75}Se_{0.25}$.

The renormalized phonon frequencies and the scattering rates are further applied to compute the temperature dependence of κ_L of SnS and the ordered $SnS_{0.75}Se_{0.25}$ along three directions using UT, which includes both the phonon population (κ_p) and coherence (κ_c) contributions from the heat-flux operator. For comparison, κ_L of SnS and the ordered $SnS_{0.75}Se_{0.25}$ calculated from NEMD simulations with our machine learning MTPs and the experimentally measured values of SnS[6] are summarized in Figure 6(a-d). A reasonable agreement of κ_L along three directions for SnS is observed between the experimental measurements[6] and our NEMD simulations, which inherently include all orders of lattice phonon anharmonicity. The κ_L^x has about 12.5% and 13.2% reductions for SnS and the order $SnS_{0.75}Se_{0.25}$, respectively, after considering fourth-order phonon scatterings at 300 K. It is apparent from Figure 6(a-b) that κ_p governs the heat transport of *Pnma*-SnS and *Pnma*-$SnS_{0.75}Se_{0.25}$ at 300 K. However, as shown in Figure 6(c-d), the κ_c becomes comparable to the κ_p for the *Cmcm* phase at 800 K, suggesting the importance of the coherence channel in describing the thermal transport of both *Cmcm*-SnS and *Cmcm*-$SnS_{0.75}Se_{0.25}$ at high temperatures. In addition, a noticeable difference of κ_L between UT and the NEMD is observed for both phases of SnS and $SnS_{0.75}Se_{0.25}$. This may be caused by non-perturbative phonon scatterings[12]. Further, we observe an average 14.7% reduction on κ_L of $SnS_{0.75}Se_{0.25}$ at 300 K by

randomizing the Se atoms in the supercell, as shown in Figure 6(b). This can be interpreted by the Klemens model[46]: $\tau_D^{-1} = \omega^4 V \sum_i f_i \left(\frac{m_i}{\bar{m}} - 1\right)^2 / (4\pi v^3)$, where V is the volume per unit atom, f_i is the concentration of species i, v is the branch-averaged sound velocity, m_i and $\bar{m}$ are the atomic mass and the average mass of species i, respectively. The disordering of the Se atoms clearly increases the phonon scattering by introducing sublattice mass disorder, resulting in a decreased κ_L. However, as shown in Figure 6(d), the difference of κ_L between the ordered and the general SQS of $SnS_{0.75}Se_{0.25}$ decreases with increasing temperature, which can be ascribed to the dominance of phonon-phonon scattering at elevated temperatures.

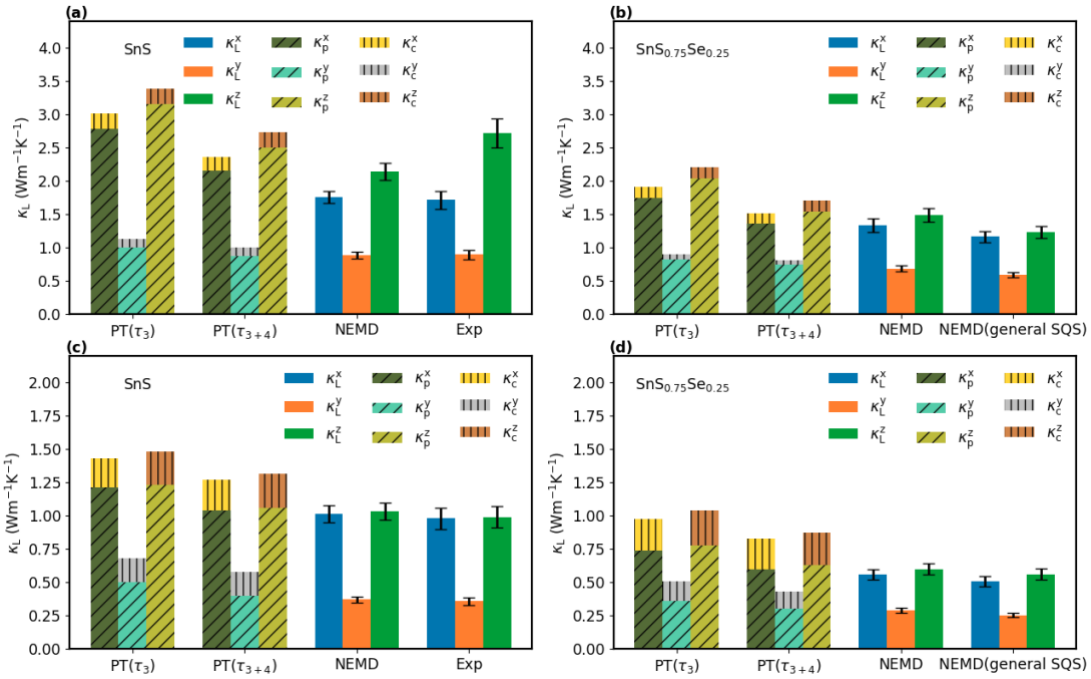

Figure 6. Lattice thermal conductivities of SnS, the ordered $SnS_{0.75}Se_{0.25}$, and the SQS of $SnS_{0.75}Se_{0.25}$ calculated from UT and NEMD at 300 K (a-b) and 800 K (c-d). The experimental values are taken from Ref.[6]. The NEMD results of SnS are taken from our previous work[47].

4. Conclusion

In summary, the anharmonic lattice dynamics and thermal transport properties of SnS and $SnS_{0.75}Se_{0.25}$ have been investigated based on PT up to quartic anharmonicity and MD simulations with first-principles-based machine learning MTPs, which are capable of reproducing the lattice evolution across the structural phase transition. We observe a

non-monotonic temperature dependence of the phonon linewidths of the Γ_4 and Y_1 modes of $SnS_{0.75}Se_{0.25}$. Our results show that the apparent κ_L reduction after Se alloying is mainly attributed to the increased phonon scattering rates of the middle-frequency phonons and the decreased group velocities of the high-frequency modes. We also find that the quartic anharmonicity and the coherence contribution are non-negligible in describing the lattice thermal transport of SnS and $SnS_{0.75}Se_{0.25}$. Furthermore, our results reveal a significant decrease of κ_L in $SnS_{0.75}Se_{0.25}$ by randomizing Se atoms in the supercell at 300 K. This work paves the way for further phonon and thermal transport engineering of SnS-based alloys.

See the Supplementary Material for details of methodology and additional calculations to support our conclusions.

N.O. and C.W. contributed equally to this work.

The authors declare that they have no conflict of interest.

This work is supported by the Zhejiang Provincial Natural Science Foundation (LR19A040001), the Research Grants Council of Hong Kong (17201019 and 17306721), and the National Natural Science Foundation of China (11874313). The authors are grateful for the research computing facilities offered by ITS, HKU.

References

1. Ghosh D, Calizo I, Teweldebrhan D, Pokatilov EP, Nika DL, Balandin AA, et al. **Extremely high thermal conductivity of graphene: Prospects for thermal management applications in nanoelectronic circuits**. *Applied Physics Letters* 2008; 92(15):151911.

2. Qu X-h, Zhang L, Mao W, Ren S-b. **Review of metal matrix composites with high thermal conductivity for thermal management applications**. *Progress in Natural Science: Materials International* 2011; 21(3):189-197.

3. Goldsmid HJ. **Theory of thermoelectric refrigeration and generation**. In: *Introduction to Thermoelectricity*: Springer; 2016. pp. 9-24.

4. Bell LE. **Cooling, heating, generating power, and recovering waste heat with thermoelectric systems**. *Science* 2008; 321(5895):1457-1461.

5. Zebarjadi M, Esfarjani K, Dresselhaus M, Ren Z, Chen G. **Perspectives on thermoelectrics: from fundamentals to device applications**. *Energy & Environmental Science* 2012; 5(1):5147-5162.

6. He W, Wang D, Wu H, Xiao Y, Zhang Y, He D, et al. **High thermoelectric performance in low-cost $SnS_{0.91}Se_{0.09}$ crystals**. *Science* 2019; 365(6460):1418-1424.

7. Wang H, LaLonde AD, Pei Y, Snyder GJ. **The criteria for beneficial disorder in thermoelectric solid solutions**. *Advanced Functional Materials* 2013; 23(12):1586-1596.

8. Wu H-j, Chen S-w, Ikeda T, Snyder GJ. **Reduced thermal conductivity in Pb-alloyed $AgSbTe_2$ thermoelectric materials**. *Acta Materialia* 2012; 60(17):6144-6151.

9. Zhao L-D, Lo S-H, Zhang Y, Sun H, Tan G, Uher C, et al. **Ultralow thermal conductivity and high thermoelectric figure of merit in SnSe crystals**. *Nature* 2014; 508(7496):373-377.

10. Wang Y, Qin B, Hong T, Su L, Gao X, Wang D, et al. **Enhanced thermoelectric perfromance in cubic form of SnSe stabilized through enformatingly alloying $AgSbTe_2$**. *Acta Materialia* 2022; 227:117681.

11. Li S, Zhang F, Chen C, Li X, Cao F, Sui J, et al. **Enhanced thermoelectric performance in polycrystalline N-type Pr-doped SnSe by hot forging**. *Acta Materialia* 2020; 190:1-7.

12. Zeng Z, Zhang C, Xia Y, Fan Z, Wolverton C, Chen Y. **Nonperturbative phonon scatterings and the two-channel thermal transport in Tl_3VSe_4**. *Physical Review B* 2021; 103(22):224307.

13. Wang Q, Zeng Z, Chen Y. **Revisiting phonon transport in perovskite $SrTiO_3$: Anharmonic phonon renormalization and four-phonon scattering**. *Physical Review B* 2021; 104(23):235205.

14. Zeng Z, Zhang C, Yu H, Li W, Pei Y, Chen Y. **Ultralow and glass-like lattice thermal conductivity in crystalline $BaAg_2Te_2$: Strong fourth-order anharmonicity and crucial diffusive thermal transport**. *Materials Today Physics* 2021; 21:100487.

15. Zhang C, Zeng Z, Sun Q, Chen Y. **Stronger three-phonon interactions revealed by molecular dynamics in materials with restricted phase space**. *Journal of Applied Physics* 2021; 130(20):205101.

16. Guo R, Wang X, Kuang Y, Huang B. **First-principles study of anisotropic thermoelectric transport properties of IV-VI semiconductor compounds SnSe and SnS**. *Physical Review B* 2015; 92(11):115202.

17. Aseginolaza U, Bianco R, Monacelli L, Paulatto L, Calandra M, Mauri F, et al. **Strong anharmonicity and high thermoelectric efficiency in high-temperature SnS from first principles**. *Physical Review B* 2019; 100(21):214307.

18. Minnich AJ, Chen G, Mansoor S, Yilbas B. **Quasiballistic heat transfer studied using the frequency-dependent Boltzmann transport equation**. *Physical Review B* 2011; 84(23):235207.

19. Hollingsworth SA, Dror RO. **Molecular dynamics simulation for all**. *Neuron* 2018; 99(6):1129-

1143.
20. Novikov IS, Gubaev K, Podryabinkin EV, Shapeev AV. **The MLIP package: moment tensor potentials with MPI and active learning**. *Machine Learning: Science and Technology* 2020; 2(2):025002.
21. Zhang D-B, Sun T, Wentzcovitch RM. **Phonon quasiparticles and anharmonic free energy in complex systems**. *Physical review letters* 2014; 112(5):058501.
22. Sun T, Zhang D-B, Wentzcovitch RM. **Dynamic stabilization of cubic $CaSiO_3$ perovskite at high temperatures and pressures from ab initio molecular dynamics**. *Physical Review B* 2014; 89(9):094109.
23. Simoncelli M, Marzari N, Mauri F. **Unified theory of thermal transport in crystals and glasses**. *Nature Physics* 2019; 15(8):809-813.
24. Kresse G, Hafner J. **Ab initio molecular dynamics for liquid metals**. *Physical Review B* 1993; 47(1):558.
25. Blöchl PE. **Projector augmented-wave method**. *Physical review B* 1994; 50(24):17953.
26. Perdew JP, Ruzsinszky A, Csonka GI, Vydrov OA, Scuseria GE, Constantin LA, et al. **Restoring the density-gradient expansion for exchange in solids and surfaces**. *Physical review letters* 2008; 100(13):136406.
27. Monkhorst HJ, Pack JD. **Special points for Brillouin-zone integrations**. *Physical review B* 1976; 13(12):5188.
28. Zunger A, Wei S-H, Ferreira L, Bernard JE. **Special quasirandom structures**. *Physical review letters* 1990; 65(3):353.
29. Glass CW, Oganov AR, Hansen N. **USPEX—Evolutionary crystal structure prediction**. *Computer physics communications* 2006; 175(11-12):713-720.
30. Plimpton S. **Fast Parallel Algorithms for Short-Range Molecular Dynamics**. *Journal of Computational Physics* 1995; 117(1):1-19.
31. Sun T, Shen X, Allen PB. **Phonon quasiparticles and anharmonic perturbation theory tested by molecular dynamics on a model system**. *Physical Review B Condensed Matter* 2010; 82(22):1707-1712.
32. Wen X, Zhu L, Cai Y, Gang Z, Li B. **Direction dependent thermal conductivity of monolayer phosphorene: parameterization of Stillinger-Weber potential and molecular dynamics study**. *Journal of Applied Physics* 2015; 117(21):214308.214301-214308.214307.
33. Wang C, Wu J, Zeng Z, Embs J, Pei Y, Ma J, et al. **Soft-mode dynamics in the ferroelectric phase transition of GeTe**. *npj Computational Materials* 2021; 7(1):1-7.
34. Wang C, Chen Y. **Highly selective phonon diffusive scattering in superionic layered $AgCrSe_2$**. *npj Computational Materials* 2020; 6(1):1-6.
35. Peierls R, Peierls RE. **Quantum theory of solids**. Oxford University Press; 1955.
36. Hellman O, Steneteg P, Abrikosov IA, Simak SI. **Temperature dependent effective potential method for accurate free energy calculations of solids**. *Physical Review B* 2013; 87(10):104111.
37. Eriksson F, Fransson E, Erhart P. **The Hiphive Package for the Extraction of High-Order Force Constants by Machine Learning**. *Advanced Theory & Simulations* 2019.
38. Xia Y, Hegde VI, Pal K, Hua X, Gaines D, Patel S, et al. **High-throughput study of lattice thermal conductivity in binary rocksalt and zinc blende compounds including higher-order anharmonicity**. *Physical Review X* 2020; 10(4):041029.
39. Ikeshoji T, Hafskjold B. **Non-equilibrium molecular dynamics calculation of heat conduction in**

liquid and through liquid-gas interface. *Molecular Physics* 1994; 81(2):251-261.
40. Rini AS. **Diffraction Pattern Simulation of Crystal Structure towards the Ionic Radius Changes Via Vesta Program**. *Journal of Technomaterial Physics* 2019; 1(2):132-139.
41. Ouyang N, Wang C, Zeng Z, Chen Y. **Anharmonic lattice dynamics of SnS across phase transition: A study using high-dimensional neural network potential**. *Applied Physics Letters* 2021; 119(6):061902.
42. Chattopadhyay T, Pannetier J, Von Schnering H. **Neutron diffraction study of the structural phase transition in SnS and SnSe**. *Journal of Physics and Chemistry of Solids* 1986; 47(9):879-885.
43. Liu H, Qian X, Bao H, Zhao C, Gu X. **High-temperature phonon transport properties of SnSe from machine-learning interatomic potential**. *Journal of Physics: Condensed Matter* 2021; 33(40):405401.
44. Eriksson F, Fransson E, Erhart P. **The Hiphive Package for the extraction of high-order force constants by machine learning**. *Advanced Theory and Simulations* 2019; 2(5):1800184.
45. Carreras A, Togo A, Tanaka I. **DynaPhoPy: A code for extracting phonon quasiparticles from molecular dynamics simulations**. *Computer Physics Communications* 2017; 221:221-234.
46. Agrawal BK, Verma G. **Lattice thermal conductivity at low temperatures**. *Physical Review* 1962; 126(1):24.
47. Ouyang N, Wang C, Chen Y. **Temperature-and pressure-dependent phonon transport properties of SnS across phase transition from machine-learning interatomic potential**. *International Journal of Heat and Mass Transfer* 2022; 192:122859.